Electrical Properties and Shrinkage of Carbonized Photoresist Films and the Implications for Carbon Microelectromechanical Systems Devices in Conductive Media

Journal of The Electrochemical Society, **152** (12) J136-J143 (2005)
0013-4651/2005/152(12)/J136/8/$7.00 © The Electrochemical Society, Inc.

Electrical Properties and Shrinkage of Carbonized Photoresist Films and the Implications for Carbon Microelectromechanical Systems Devices in Conductive Media

Benjamin Y. Park,[a] Lili Taherabadi,[b] Chunlei Wang,[c] Jim Zoval,[c] and Marc J. Madou[d]

[a]*Mechanical and Aerospace Engineering,* [b]*Materials Science and Engineering,* [c]*Mechanical and Aerospace Engineering, and* [d]*Mechanical and Aerospace Engineering and Biomedical Engineering, University of California, Irvine, Irvine, California 92697-3975, USA*

Recent advances in fabricating 3D micro- and nanostructures using carbon microelectromechanical systems, or C-MEMS, has opened up a wide variety of new and exciting applications. The development of 3D C-MEMS has been catapulted forward by the use of transparent, high-viscosity resists such as SU-8. The electrical characteristics and shrinkage of various thickness carbon films derived from SU-8 and AZ P4620 are quantified and discussed in the context of the decomposition and carbonization mechanisms of epoxy and phenolic resins. Measurements obtained reveal a thickness dependence of the resistivity at lower carbonization temperatures but not much dependence at 1000°C. Possible explanations for this low-temperature thickness dependence are given. The electrical characteristics of carbon films obtained from both types of photoresists carbonized at 1000°C are very similar to that of glassy carbon. Simulations have been carried out to demonstrate the importance of the carbon resistivity for C-MEMS devices when used in conductive media. A method for simple optimization and verification of C-MEMS device designs for use in conductive media is introduced.
 [DOI: 10.1149/1.2116707]

Manuscript submitted May 12, 2005; revised manuscript received August 8, 2005. Available electronically November 1, 2005.

Carbon chemistry is uniquely complex and versatile due to the ability of carbon atoms to form long chains and because of the changes in chemical and physical properties that occur due to the different bond types between carbon atoms. The versatility of carbon materials comes from the three different bonds that carbon atoms can make: sp^1, sp^2 (graphitelike), and diamondlike (sp^3). Since ancient times, man has been creating carbon from various precursors.[1] One method of creating artificial carbon is through heat-treatment of hydrocarbons. The formation of carbon from gaseous precursors was an undesired side reaction in petrochemistry in the past,[2] but carbonization of organic materials has become a valuable method of obtaining various carbons. When organic materials are exposed to high temperatures in an inert atmosphere, the materials decompose into simpler compounds (referred to as chain scission, pyrolysis, thermolysis, or thermal cracking). Some of these intermediate species may then react to form a solid carbon char (C_∞). Chemisorption of gas-phase organics (especially benzene) is thought to be the dominant carbon-forming mechanism for chemical vapor deposition (CVD) of pyrocarbons.[2-8] The predominant carbonization mechanisms for in situ carbonization of polymers is cross-linking, side-chain elimination (including dehydrogenization), and side-chain cyclization of polymers.[9,10] Although the term pyrolysis has been used in the literature to refer to the chain scission of organic compounds as well as to the formation of solid carbon from organic compounds, the term carbonization is used in this paper to refer to the creation of solid carbon (C_∞) through processes including scission. Heat-treatment (usually above 2600°C) of these pyrocarbons, in conjunction with application of pressure, can cause the material to exhibit long-range graphitic order in a process termed graphitization.[1] Pyrocarbons and highly ordered pyrolytic graphites (HOPG) obtained through the carbonization process have played an important role in multiple fields including electrochemistry,[11] energy conversion,[12] and biomedicine (implants and artificial heat valves).[13,14]

Recently, the marriage of carbonization techniques with photolithography technology has enabled fine patterning of carbon films.[15-19] The patterning and formation of these photoresist-derived carbon films in the past has been limited to thin films because of (*i*) the low UV transparency of the photoresists used and (*ii*) the cracking and peeling of thick films. It has been shown recently that 3D high-aspect-ratio carbon structures can be made from patterned thick SU-8 negative photoresist (Microchem, Newton, MA) layers.[20] SU-8 negative photoresist is a high-transparency UV photoresist that enables creation of LIGA-like structures using traditional UV photolithography. The geometry during carbonization is preserved due to the fact that the glass transition temperature (T_g) of the material rises as it is heated because the material itself is changing from SU-8 photoresist to carbon. The melting point of carbon is much higher (>3500°C) than that of cross-linked SU-8. The temperature ramp rate is controlled such that the temperature in the oven is always lower than the glass transition temperature of the photoresist/carbon. This is done by slowly heating the sample up at a rate of 10°C/min. There is some shrinkage that occurs during the carbonization process, but because the shrinkage during the carbonization process is isometric, the shape of the original photoresist structures is preserved, albeit smaller. The details of the fabrication process are beyond the scope of this paper, and are detailed in separate papers.[20,21] The capability of creating micro- and nanoscale 3D carbon structures has opened up a wide range of new applications for pyrolytic carbon including microbatteries,[22] glucose sensors, supercapacitors, biofuel cells, dielectrophoretic electrode arrays for micromanipulation of micro- and nanoparticles,[23] electrodes for biorecording/stimulation, and electrode arrays for DNA hybridization and detection. Advantages of devices fabricated using carbon microelectromechanical systems (C-MEMS) technology include the potential for crafting very small structures, a very wide electrochemical stability window, the reproducibility of the material due to the high quality of the precursor polymers, very fast electrode kinetics for simple redox systems, excellent biocompatibility, chemical inertness, good thermal conductivity, dimensional and mechanical stability, low cost, and low weight.[20,24]

The applications of C-MEMS devices can largely be divided into two categories: mechanical and electrical/electrochemical. The mechanical properties of C-MEMS carbon are currently being quantified and are of great interest, but most of the current applications of the C-MEMS devices have been electrical/electrochemical in nature. Ranganathan et al.[11] have established that electrochemical properties of AZ P4330 photoresist-derived C-MEMS carbon are comparable to that of glassy carbon. The resistivity of the carbon that is formed through the C-MEMS process is an important parameter for all electrical and electrochemical uses of C-MEMS devices. For example, if the C-MEMS process is used to create battery interconnects and/or electrodes for a Li-ion battery, the resistivity of the carbon may have a significant impact on the internal resistance of the battery. Typical solid electrolyte Li-ion batteries have only ~400 mΩ of internal resistance, and if the internal resistance due to the carbon electrodes contributes significantly to the total internal resistance, the resulting

Table I. The processing parameters for the various resist films.

Sample	Photoresist type and viscosity	Wafer preparation	Spin steps	Spin speed (time)
AZ″	AZ 4620	Dehydration for 2–10 min at 95°C	Single	4000 rpm (30 s)
1.5 μm″	SU-82	Dehydration for 2–10 min at 95°C	2 step	500 rpm (12 s) → 3000 rpm (30 s)
5 μm″	SU-82	Dehydration for 2–10 min at 95°C	2 step	500 rpm (12 s) → 1000 rpm (30 s)
15 μm″	SU-85	Dehydration for 2–10 min at 95°C	2 step	500 rpm (12 s) → 1000 rpm (30 s)
25 μm″	SU-8 25	Dehydration for 2–10 min at 95°C	2 step	500 rpm (12 s) → 2000 rpm (30 s)

Sample	Photoresist type and viscosity	Soft bake temperatures (time)	Broadband UV exposure dose	PEB temperatures (time)	Initial thickness (μm)
AZ″	AZ 4620	95°C (2 min)	N/A	N/A	7.35
1.5 μm″	SU-8 2	65°C (1 min) → 95°C (1 min)	91.25 mJ/cm2	65°C (1 min) → 95°C (1 min)	1.29
5 μm″	SU-8 2	65°C (1 min) → 95°C (3 min)	98.55 mJ/cm2	65°C (1 min) → 95°C (1 min)	3.23
15 μm″	SU-8 5	65°C (2 min) → 95°C (5 min)	197.10 mJ/cm2	65°C (1 min) → 95°C (2 min)	11.70
25 μm″	SU-8 25	65°C (3 min) → 95°C (7 min)	219.00 mJ/cm2	65°C (1 min) → 95°C (3 min)	23.06

Li-ion battery will have a very small power output. Since the impendence of a C-MEMS device is determined by the design of the device and the resistivity of the carbon, a priori determination of the electrical characteristics is required to ensure that a particular design will work for a specific application. In the case of most electrochemical devices, the electrical potential is used to drive the reaction of interest. Therefore, it is essential that the voltage drop occurs across the electrode–electrolyte interface, not over the electrolyte or inside the electrodes or the connections to the electrodes.

Although the sheet resistance of photoresist-derived carbon has been measured at different temperature,[15-19] and a relationship between resist tone and the properties of the derived carbon has been hypothesized by Singh et al.,[19] the effect of different resist thickness on the carbonization process has not been quantified. This is mostly due to the cracking and peeling of the carbon exhibited in past attempts using thick photoresist layers.[19]

In this paper, the electrical property changes and shrinkage of AZ P4620 (AZ Electronic Materials, Somerville, NJ) and SU-8 photoresists carbonized at different temperatures ranging from 600–1000°C are examined. AZ P4620 is a cresol novolak resin-based thick film positive photoresist.[25] AZ P4620 is of particular interest in MEMS because of its ability to create films with thicknesses of over 60 μm, and because it can be fully cross-linked to act as a dielectric or become a permanent part of a device. After analysis of the experimental data, simulation results showing the significance of the resistivity of C-MEMS carbon for applications in conductive media are presented.

Experimental

Preparation of the photoresist films.— All experiments were performed in the UCI Integrated Nanosystems Research Facility (INRF). The INRF is a class 1000/10,000 clean room with class 100 work areas. The humidity within the lithography rooms is controlled to be between 45 and 55% RH. AZ P4620 and SU-8 photoresist were applied to 4 in. diameter 5000 Å SiO_2/Si wafers. The manufacture-recommended recipes for 1.5, 5, 15, and 25 μm layers were followed for the SU-8 layers.[26] AZ P4620 is a positive photoresist. For positive photoresists, the resist is typically cross-linked during the initial bake. Exposure to UV reduces the amount of cross-linking, making the exposed resist more soluble in the developer solution. In negative photoresists, cross-linking is induced during UV exposure and the following bake step. No exposure or postexposure baking steps were done for the AZ P4620 films before carbonization in the furnace. Exposure and postexposure baking steps were performed in the case of the SU-8 films to induce cross-linking.[26] The processing conditions for the application of the resist layers are given in Table I. For all of the samples, a small portion of the wafer was developed to be free of photoresist to allow simple measurement of film thickness.

Four samples of the same type (same thickness and photoresist type) were cleaved from a single wafer to insure that the thicknesses of the samples were identical. To keep the error due to edge effects in resistivity and sheet resistance measurements smaller than 1%, a sample with a diameter (or width) of approximately. 40 times the probe tip spacing is required (~0.9945 correction factor).[27] The probe tip spacing for the four-point probe tool used is 1 mm. A circle with a 4.2 cm diameter just fits inside a 4 in. quarter wafer; thus, cleaving the wafer into smaller pieces was not an option. The actual thickness obtained after soft baking and development of the AZ P4620 layers was 7.34 μm (measured with the Tencor Alpha-Step 200 surface profilometer). The thicknesses obtained after postexposure bake and development for the SU-8 films were 1.20, 3.23, 11.70, and 23.06 μm. The AZ P4620 samples are referred to as the AZ samples, and the SU-8 samples are referred to by the thickness recipe that was followed to spin on the photoresist: the 1.20 μm thick SU-8 samples are referred to as "1.5 μm," the 3.23 μm thick samples as "5 μm," the 11.70 μm thick samples as "15 μm," and the 23.06 μm thick samples as "25 μm." The 1.5 and 5 μm samples were made from SU-8 2, the 15 μm samples from SU-8 5, and the 25 μm samples were made from SU-8 25. Since five samples were required for each sample type, additional quarter wafers were coated using the same recipes. These samples correspond to the samples carbonized at 600°C. Although the initial height measurement for each type of sample that was carbonized at 700–1000°C was identical, the initial thicknesses of the samples carbonized at 600°C were slightly different because of variability in the resist spinning setup. The heights of the samples carbonized at 600°C shown in Fig. 5 were scaled according to the initial thicknesses of the samples compared to that of the other samples.

Carbonization of the photoresist films.— Five quarter wafers with AZ P4620 photoresist applied at a thickness of 7.34 μm, and SU-8 photoresist applied at the thicknesses of 1.2, 3.23, 11.7, and 23.06 μm (measured with the Tencor Alpha-Step 200 surface profilometer) were heated in an open-ended quartz furnace. A two-step heating protocol was used with a hard baking step (to ensure complete hardening of the photoresist) followed by the actual carbonization bake. The hard bake consisted of raising the temperature of the furnace at a rate of 10°C/min and holding the temperature at 300°C for 30 min. The carbonization bake directly followed the hard bake.

In this step, the furnace temperature was raised 10°C/min to the desired carbonization temperatures of 600, 700, 800, 900, and 1000°C and held at that temperature for 1 h. The samples were then allowed to cool for 9 h. N_2 gas was flowed at 2000 standard cubic centimeters per min (sccm) during the hard bake and the cooling steps. A 95% N_2/5% H_2 mixture (forming gas) was used during the 1 h bake at the final carbonization temperature to create a reducing atmosphere void of oxygen.[11]

Thickness measurement.— Thickness measurements were performed on each sample with the Tencor Alpha-Step 200 surface profilometer. Multiple measurements (2–4) were carried out on each sample to ensure quality of data. Even though the standard deviation is shown in the graphs, the standard deviation cannot be reasonably calculated based on two to four measurements.

Resistivity and sheet resistance measurements.— A Lucas Signatone model SYS-301-4 four-point probe connected to a Keithley 2400 SourceMeter inside a custom-made dark box was used to measure the sheet resistance and resistivity. The thin sheet assumption was valid for our samples because the thicknesses of the carbon films ($\leqslant$5.53 μm) were much smaller than the probe spacing in the four-point probe (1 mm).

The thin sheet equation used for calculation of sheet resistance is[28]

$$R_s = \frac{\pi}{\ln 2}\left(\frac{V}{I}\right) \quad [1]$$

where R_s = sheet resistance, V = voltage applied to the inner probes, I = current measured at the outer probes.

The resistivity was calculated by multiplying the sheet resistance with the thickness of the carbon layer[28]

$$\rho = R_s t \quad [2]$$

where ρ = resistivity, t = thickness of the film.

Multiple sheet resistance measurements were carried out (2–10 measurements) on each sample to ensure data integrity. The applied currents ranged from 1 μA to 4 mA. For each measurement a different current was applied, and the sample was rotated. Different currents were applied to make sure that the measurements were made in the linear region of the I/V curves. The samples were rotated to ensure that there was no anisotropy in the resistivity of the films (due, for example, to graphitization). All measurements were carried out in a temperature-controlled clean room environment. The measurements were all performed within a week from carbonization (usually within a day). Duplicate measurements for some samples were made 3 weeks after carbonization of the films, and no significant difference was measured.

Resistivity is a materials property, and the conversion of sheet resistance to resistivity assumes uniformity of material.

Results

All samples were black, brittle, and had a high luster. Most of the samples were smooth and uniform without any cracking or detachment from the substrate, but the 25 μm films carbonized at 600 and 700°C exhibited extensive cracking and peeling throughout the sample. No sheet resistance data could be obtained from these samples.

The results from the sheet resistance measurements for the five different samples carbonized at five different temperatures are shown in Fig. 1 and 2. The sheet resistances of samples carbonized at 600°C were too high for the measurement setup to accurately measure. A log scale was used for both of these graphs because of the wide range of sheet resistances that was measured.

The resistivities calculated from the sheet resistances and from thickness measurements are shown in Fig. 3 and 4. These values assume homogeneity of the carbon material in the films.

The height measurements of the photoresist films are depicted in Fig. 5. The first height measurement was performed after postexposure bake (PEB) and development for the SU-8 samples. Although no postexposure bake was performed on the AZ P4620 samples, and the initial height data were obtained after the development of the resist, the initial measurement points for the AZ P4620 samples are labeled as "after PEB" in the figure for convenience. The plots for the normalized mean thicknesses of the carbon films obtained from AZ P4620 and SU-8 resists as a function of carbonization temperature are shown in Fig. 6.

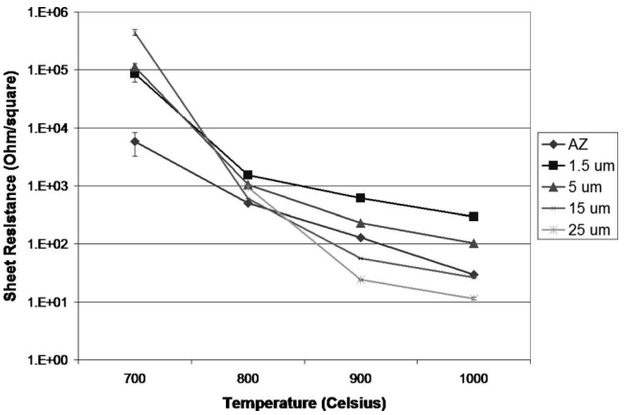

Figure 1. The sheet resistance of carbon films obtained from AZ P4620 photoresist and various-thickness SU-8 films after 1 h of heat-treatment at different temperatures. (Each line represents a different resist type or thickness.) Error bars represent ±1 SD. Some error bars are too small to be seen.

The mean film thickness, resistivity, and sheet resistance data are presented in Table II.

Discussion

For both resist films, most of the shrinkage happens before 600°C, but no significant shrinkage happens at higher temperatures. Significant change in sheet resistance was observed at temperatures between 600 and 1000°C. At 1000°C, carbon film resistivities obtained from all samples, regardless of resist type or thickness, were similar ($5.330 \pm 0.574 \times 10^{-5}$ Ω m).

There was no significant shrinkage difference for AZ P4620 films carbonized at temperatures between 600 and 1000°C. All of the AZ P4620 films shrank to 22.6 ± 0.4% of their original thicknesses, and all of the shrinkage occurred at temperatures below 600°C. There was a slight further shrinkage for the SU-8 films at temperatures

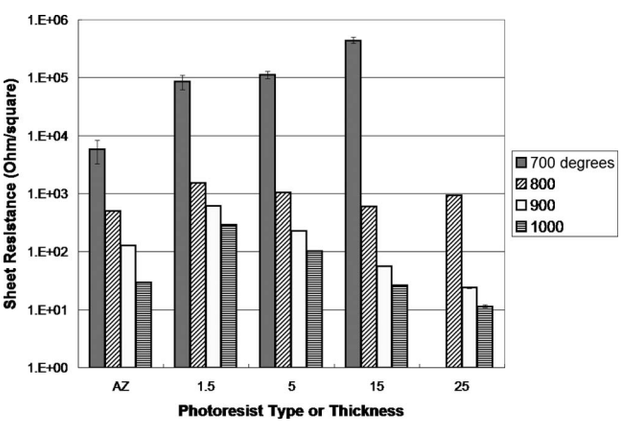

Figure 2. The sheet resistance of carbon films obtained from AZ P4620 photoresist and various-thickness SU-8 films after 1 h of heat-treatment at different temperatures. (Each line represents a different carbonization temperature.) Error bars represent ±1 SD. Some error bars are too small to be seen.

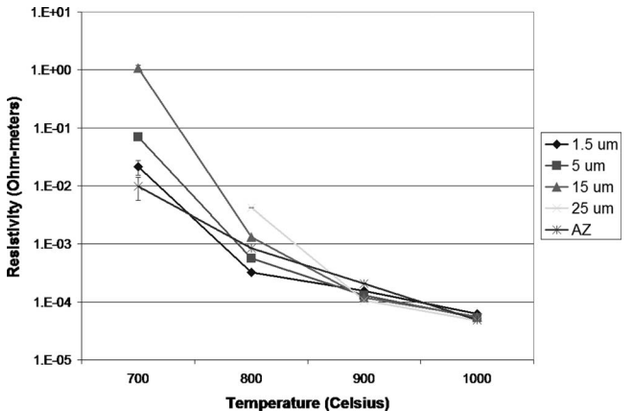

Figure 3. The resistivity of carbon films obtained from AZ P4620 photoresist and various-thickness SU-8 films after 1 h of heat-treatment at different temperatures. The values were calculated from sheet resistance and thickness measurements assuming homogeneity of material. (Each line represents a different resist type or thickness.) Error bars represent ±1 SD. Some error bars are too small to be seen.

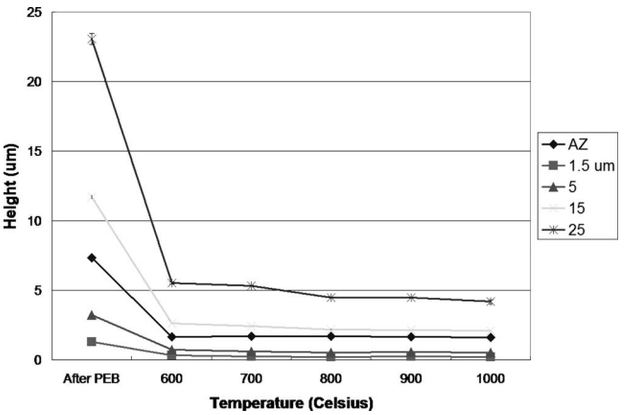

Figure 5. The height measurements of carbon films obtained from AZ P4620 photoresist and various-thickness SU-8 films after 1 h of heat-treatment at different temperatures. (Each line represents a different resist type or thickness). Note: No PEB was done for the AZ P4620 samples. Error bars represent ±1 SD. Some error bars are too small to be seen.

above 600°C (from 23.0 ± 1.0% of the original thickness at 600°C to 17.2 ± 1.0% at 1000°C), but, as in the case of the AZ P4620 films, most of the reduction in thickness occurred before 600°C. Because the shrinkage of the films can be attributed to the loss of gases, it can be inferred that most of the reactions that produce carbon and oxygen-containing gases occur at temperatures lower than 600°C. Kostecki et al.[18] found indeed that most of the reduction in the oxygen content of OIR-897 photoresist happens at temperatures below 600°C. The vertical shrinkage we observe here is similar to those recorded for SU-8 derived films by Singh and colleagues.[19] The shrinkage behavior during carbonization is different for nitrogen containing polymers such as polyimide films, where Meng et al.,[29] for example, have observed that, for Novax polyimide films, although there is an initial weight reduction between the temperatures of 450 and 600°C, a second reduction in weight occurs at temperatures above 800°C. They attribute the second weight change to N_2 evolution.

SU-8 photoresist (after evaporation of solvent) is mostly composed of bisphenol A-epichlorohydrin-formaldehyde copolymer (an epoxy/phenolic resin), and the base polymer for AZ P4620 is *m*-cresol-*p*-cresol-formaldehyde-xylenol copolymer (a cresol novolak resin). Both resists are based on phenolic resins. Studies of the decomposition of epoxy and phenolic resins have been done in the past.[9,10,30,31] It has been reported that epoxylated resins are less stable than other phenolic resins, and that the decomposition of epoxy resins follows several concurrent paths yielding mostly phenolic compounds (phenol, cresols, C_2H_5 phenols, isopropylphenol, isopropenylphenol, bisphenol-A, etc.).[9,30] Most nonepoxylated phenolic resins start decomposing at ~300°C by scission of methylene-benzene ring bonds. At 360°C, C_3 product gases begin to escape. At temperatures above ~450°C, solid carbon (C_∞) starts forming and carbon oxides and water vapor are evolved. Aromatic products start degassing at 500°C, and at ~800°C, ring scission starts to occur (methane and more carbon oxides are released). For both epoxylated and nonepoxylated phenolic resins, most of the degassing occurs at temperatures below 600°C; this agrees with our experimental observation that most of the shrinkage in both SU-8 and AZ P4620 resist films happens at temperatures below 600°C. Thermodynamic calculations done by Benzinger and Hüttinger show that, at 900–1000°C, any hydrocarbon will be almost completely decomposed into hydrogen and carbon.[2,8] The fact that raising the carbonization tempera-

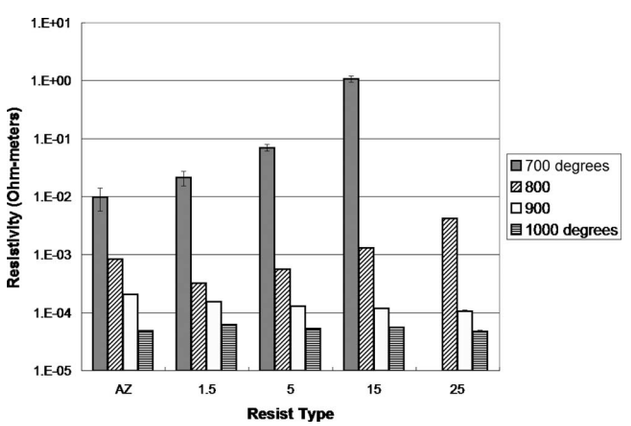

Figure 4. The resistivity of carbon films obtained from AZ P4620 photoresist and various-thickness SU-8 films after 1 h of heat-treatment at different temperatures. The values were calculated from sheet resistance and thickness measurements assuming homogeneity of material. (Each line represents a different carbonization temperature.) Error bars represent ±1 SD. Some error bars are too small to be seen.

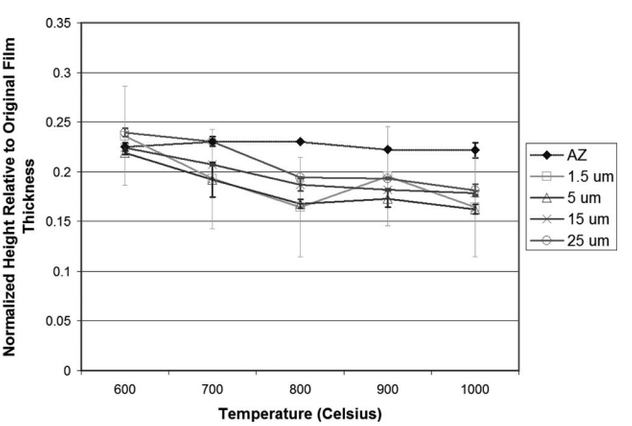

Figure 6. The normalized mean height measurements of carbon films obtained from AZ P4620 photoresist and various-thickness SU-8 films after 1 h of heat-treatment at different temperatures. (Each line represents a different resist type or thickness.) The film thicknesses were normalized to the original thickness for each sample. Error bars represent ±1 SD. Some error bars are too small to be seen.

Table II. Table of the mean thickness, resistivity, and sheet resistance data.

Mean film thickness at different carbonization temperatures (μm)					
	AZ	1.5	5	15	25
Initial	7.35	1.29	3.23	11.70	23.06
600	1.66	0.30	0.71	2.63	5.53
700	1.69	0.25	0.62	2.42	5.32
800	1.69	0.21	0.54	2.19	4.48
900	1.64	0.25	0.56	2.13	4.46
1000	1.63	0.21	0.52	2.09	4.18
Mean resistivity at different carbonization temperatures (Ω-m)					
	AZ	1.5	5	15	25
700	9.80×10^{-3}	2.12×10^{-2}	6.98×10^{-2}	1.07	N/A
800	8.39×10^{-4}	3.23×10^{-4}	5.60×10^{-4}	1.32×10^{-3}	4.19×10^{-3}
900	2.09×10^{-4}	1.54×10^{-4}	1.29×10^{-4}	1.19×10^{-4}	1.07×10^{-4}
1000	4.82×10^{-5}	6.17×10^{-5}	5.36×10^{-5}	5.52×10^{-5}	4.77×10^{-5}
Mean sheet resistance at different carbonization temperatures (Ω/□)					
	AZ	1.5	5	15	25
700	5.79×10^{3}	8.53×10^{4}	1.13×10^{5}	4.43×10^{5}	N/A
800	4.96×10^{2}	1.53×10^{3}	1.03×10^{3}	6.02×10^{2}	9.34×10^{2}
900	1.28×10^{2}	6.13×10^{2}	2.31×10^{2}	55.9	24.1
1000	29.6	2.92×10^{2}	1.02×10^{2}	26.4	11.4

ture to 1000°C causes the SU-8 films to continue to shrink, along with the fact that the sheet resistance and the resistivity curves for the SU-8 derived carbon are steeper than the those for AZ P4620-derived films, leads us to believe that the SU-8-derived films are less carbonized than the films derived from AZ P4620. We believe that increasing the carbonization temperature beyond 1000°C or increasing the heat-treatment time will further decrease the sheet resistance, resistivity, and thickness of the SU-8 derived carbon films. Future experiments at higher temperatures will be needed to find the temperature/time where SU-8 films are completely carbonized.

We have not yet determined the effect of the forming gas (5% H_2/95% N_2) on the carbonization process. The forming gas atmosphere was chosen to insure that there was no residual oxygen in the furnace or in the carbon formed. It is interesting that Lyons et al.[10] have observed an increase in shrinkage when using H_2 instead of N_2 as the inert atmosphere during carbonization, which they attribute to the increased formation of hydrocarbon by-products in a H_2 atmosphere. The resistivities measured at 1050°C were similar and, for the most part, independent of atmosphere.

The resistivity of the photoresists tested ranged from that of insulating (out of range) to $4.769 \pm 0.250 \times 10^{-5}$ Ω m (semimetal range) in the case of the 25 μm sample carbonized at 1000°C. There is a large change in resistivity between the temperatures of 600 and 900°C. If the hydrogen evolution temperature of the investigated resist films is similar to that of Novax films, this would correspond to the temperature at which H2 gas is evolved.[29] The drop in H/C ratio observed between 700 and 1100°C for different carbon films derived from novolak resin and epoxy novolak resin[17] supports this hypothesis. The thicker layers of SU-8-derived carbon are more resistive at lower carbonization temperatures (700–800°C), but they tend to be slightly more conductive than thinner layers at higher temperatures (900–1000°C). The resistivities of both photoresists, regardless of thickness or resist tone, were almost identical after heat-treatment at 1000°C ($5.330 \pm 0.574 \times 10^{-5}$ Ω m). We suppose this is because both resists consist mostly of phenolic resin. We are convinced that the resist chemical makeup, not necessarily the resist tone (Singh et al.[19]), is the factor determining the final properties of the resist-derived carbon.

At least two theories may explain the thickness dependence of SU-8-derived films at lower temperatures: (*i*) There may be a considerable difference in electrical properties near the surface of the films compared to those at the bottom of the films. Concentration gradients of the radicals and product gases in the carbon films formed due to removal of gaseous products at the surface during heat-treatment may cause the electrical properties to differ with distance from the top surface. (*ii*) The film thickness may affect the rate of carbonization. Thick layers impede efficient degassing of the various hydrocarbons and carbon oxides, slowing the increase of the relative amount of carbon in the film. Further investigation is required to determine the exact carbonization mechanisms of SU-8 and AZ P4620 photoresists.

Carbonization of cross-linking plastics is believed to yield mostly nongraphitic carbon.[32] In addition, phenol-formaldehyde resins are known to form glassy carbon.[31] We thus expected the electrical behavior of the carbonized SU-8 and AZ P4620 resists to resemble that of glassy carbon. The various resistivities of different carbons are given in Table III. The resistivity values measured for the SU-8 and AZ P4620 films carbonized at 1000°C ($5.330 \pm 0.574 \times 10^{-5}$ Ω m) were indeed very similar to typical values measured for vitreous (glassy) carbon (most references give a resistivity value of $\sim 5 \times 10^{-5}$ Ω m), pyrolyzed carbon, and photoresist-derived carbon.

The single low sheet resistance data point at 600°C for carbon films derived from AZ P4330 photoresist (lower than that at 700°C)[11,16] was not observed for the carbonized SU-8 and AZ P4620 films. The resistivities found for SU-8-derived carbon film by Singh et al.[19] are approximately one order of magnitude higher than the values obtained in this paper.

Significance of the Resistivity of C-MEMS Carbon for C-MEMS Applications in Conductive Media

As mentioned in the introduction, the resistance of carbon electrodes and interconnects plays a crucial role in determining the voltage distribution between the carbon and the conductive medium. In most cases, reducing the ohmic loss (voltage drop) within the carbon structures is advantageous. Finite element simulations were performed using Femlab 3.0a multiphysics modeling software (Comsol, Stockholm, Sweden). Up to the present, the interconnects in C-MEMS devices have mainly been made of C-MEMS carbon because of ease of fabrication.[21] A 4 × 4 parallel-addressed electrode array with 50 μm diameter high-aspect-ratio electrodes and 20 μm high interconnect lines was chosen to be modeled due to the relative simplicity of the geometry as well as the similarity to C-MEMS devices currently being researched for use in many different applications including C-MEMS dielectrophoretic trap arrays,[23] microbatteries,[22] and neuronal probes. Figure 7 shows an overall

Table III. Resistivity measurements from various carbons.

Carbon type	Precursor	Resistivity and heating temperature
Pyrolyzed graphite flakes[a]	Benzene, pyrazine, biphenyl naphthalene, clorobenzene bromobenzene	$(3.33–5.0) \times 10^{-5}$ Ω m (850°C) 6.67×10^{-7} to 1.1×10^{-6} Ω m (2600°C)
Compounded pure carbon[b]	N/A	$(3.1–8.1) \times 10^{-5}$ Ω m
Electrode graphite[b]	N/A	9×10^{-6} to 1.1×10^{-5} Ω m
Pure graphite[b]	N/A	8×10^{-6} to 1.3×10^{-5} Ω m
Vitreous carbon[b]	N/A	$(1–8) \times 10^{-5}$ Ω m
Natural graphite and highly ordered pyrolytic graphite (HOPG)[c]	N/A	4×10^{-6} Ω m in the basal plane
Pyrolyzed carbon[d]	Phenol-formaldehyde resin	$(1.3–4.2) \times 10^{-4}$ Ω m (800°C) 2.0×10^{-5} to 4.0×10^{-4} Ω m (1050°C)
Graphite fibers[e]	benzene	2.7×10^{-6} Ω m (2500°C) in the basal plane 7.0×10^{-7} Ω m (2800°C) in the basal plane 6.5×10^{-7} Ω m (3000°C) in the basal plane 2.2×10^{-7} Ω m (3500°C) in the basal plane
Photoresist-derived carbon[f]	AZ 4330 positive photoresist	5.1×10^{-5} Ω m (1050°C): estimated assuming 1.0 μm thickness of film
Photoresist-derived carbon[g]	HPR-206 novalak resist	$\sim 1 \times 10^{-5}$ Ω m (1050°C) $\sim 1 \times 10^{-4}$ Ω m (800°C) $\sim 1 \times 10^{-3}$ Ω m (700°C) ~ 2 Ω m (600°C)
Photoresist-derived carbon[h]	SU-8, polyimide	$(5–7) \times 10^{-4}$ Ω m (1000°C)
Pyrolyzed carbon[i]	Poly(furfuryl alcohol)	$\sim 1 \times 10^{-4}$ Ω m (1100°C)
Pyrolyzed carbon[j]	Polyacrylonitrile	$\sim 2 \times 10^{-5}$ Ω m (1020°C)
Pyrolyzed carbon[k]	Organic film	$\sim 4 \times 10^{-5}$ Ω m (1020°C)
Sputtered carbon[l]	N/A	3.5×10^{-4} Ω m

[a] Reference 34.
[b] Reference 35.
[c] Reference 36.
[d] Reference 10.
[e] Reference 37.
[f] Reference 11.
[g] Reference 15.
[h] Reference 19.
[i] Reference 38.
[j] Reference 39.
[k] Reference 40.
[l] Reference 41.

schematic of the design used in the simulations and a close-up view of the electrodes of an actual C-MEMS device. The particular device shown in the top right of Fig. 7 was used in dielectrophoretic separation experiments (unpublished results). Even though the number of electrodes was greatly reduced in the Femlab model (from a 10×10 array to a 4×4 array), Femlab was not able to process the design shown in Fig. 7 because of the complex 3D geometry. Simplification of the design was required. We assumed that most of the resistance drop occurs along the long contact lines, and that the resistance drop within the short electrodes is negligible. Additionally, even though the contact pads are usually accessed outside of the conductive media, the pads were modeled within the conductive media to further simplify the model. All simulations were done in 3D to accurately simulate the effects of conductive media on top of such a device. Figure 8 shows a close-up view of the electrode area for the simplified simulation model. The size of the whole device is approximately 1.2×1.2 cm.

For all of the experiments, effects due to the double layer and migration of ions in a fluid are ignored. Capacitance due to the double layer increases the impedance in the case of ac voltages applied in a liquid, and if dc voltages are applied in a solution, migration of ions affects the electric field distribution within the medium. The simulations represent the best-case scenario for the magnitude of the voltage seen by the conductive media. The simulation results are useful because it can reveal whether a device design can be used for a certain application. If the conductive medium is a solid, such as in the case of the solid electrolyte Li-ion battery, the simulation results will be closer to the actual values.

To illustrate how conductivity of the media can influence the voltage drop in the carbon interconnects, we first compare the simulation results for SU-8 carbonized at 900°C (1.072×10^{-4} Ω m) submersed in a low conductivity medium (typical DI water with

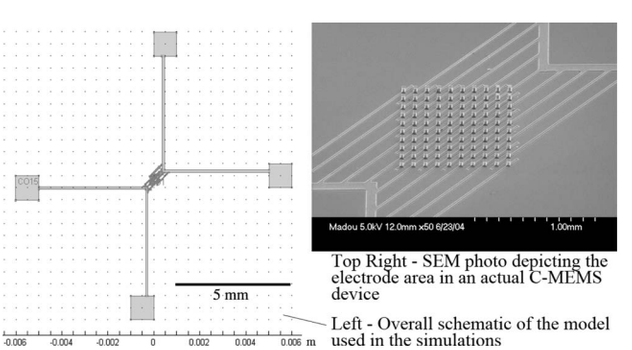

Figure 7. Overall schematic of the 3D model before simplification (left) and the close-up view of the electrode area (right).

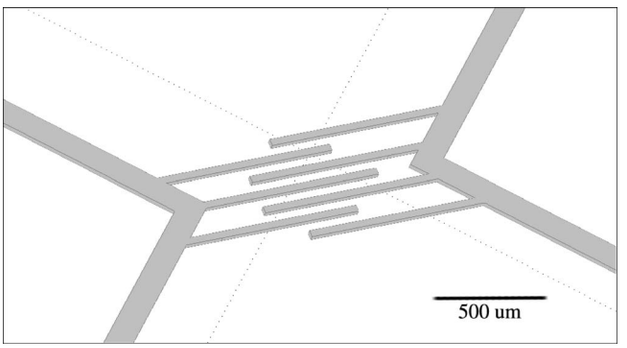

Figure 8. The close-up view of the electrode area for the simplified simulation model used in all of the simulations. Because most of the resistance is due to the interconnect layer, the postelectrodes are not taken into account during the simulation.

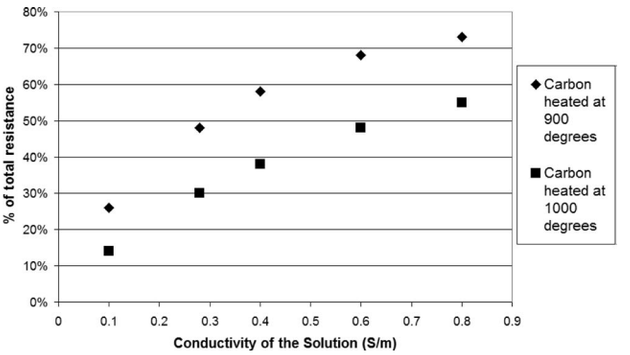

Figure 10. The percentage of the total resistance between the contact points that is attributable to the carbon interconnects. (The percentage of the voltage drop that occurs within the carbon contact lines.)

conductivity of 10^{-4} S/m) vs the same structure submersed in a conductive medium with conductivity of 0.8 S/m. A voltage of ±5 V (10 V total) was applied to the ends of the left and right contact pads. Figure 9 shows a close-up view of the simulated electrical potential surface plots for the top of the interconnects underneath the electrodes. From Fig. 9, there is no noticeable voltage drop in the carbon in low conductivity media (typical DI water), but there is a substantial voltage drop within the carbon (3.6 V for each side) for the structure immersed in the 0.8 S/m medium.

Simulations were run with varying parameters of carbon resistivity (ρ for carbon heat treated at 900°C = 1.072×10^{-4} Ω m and ρ for carbon heat treated at 1000°C = 4.769×10^{-5} Ω m) and conductive media conductivity (0.1–0.8 S/m). The percentage of the voltage loss within the carbon interconnects as compared to the total voltage loss was calculated for each simulation. This number also represents the percentage of the carbon interconnect resistance relative to the total resistance between the two contact points (where the voltage is applied). These data are shown in Fig. 10. The conductivities between 0.1 and 0.8 S/m were chosen because they represent typical conductivities of cell culture medium, and because the conductivity of the electrolyte in a typical solid–electrolyte Li-ion battery is approximately. 0.28 S/m.[33] Even though the resistivity of the carbon heat treated at 900°C is twice that of the carbon treated at 1000°C, the small difference has a surprisingly large impact. For example, if 10 V were applied to the contact points of the simulated device fabricated from 900°C carbon in a 0.28 S/m medium, only 52% of the voltage (4.2 V) would be applied to the electrode array in the middle of the device. Seventy percent of the voltage (6.2 V) would be applied in the case of 1000°C carbon. Figure 11 illustrates the different voltage drops in the carbon for C-MEMS interconnects pyrolyzed at 900 and 1000°C immersed in a 0.28 S/m solution. Computer simulations revealed that the resistance between each contact pad and the electrodes is ~600 Ω for carbon heated at 900°C and ~270 Ω for carbon heated at 1000°C. To reduce resistance for resistance-sensitive applications, metal interconnects, graphitized carbon films, or novel C-MEMS materials such as carbon derived from doped polymeric precursors must be used.

Using a simple series resistance electrical model, where two resistors represent the C-MEMS structures and a resistor represents the conductive medium, the whole system can be transformed into a single equation. We have done this for the simulated example system to show that a detailed graph (shown in Fig. 12) can be obtained from these simulation data shown in Fig. 10. The equation that represents the electrical properties of the simulated system is given below, and the resulting graph is shown in Fig. 12. The simulation data points from Fig. 10 are overlaid on Fig. 12 to show that the data fit well. The coefficients for the equation were calculated from the simulation results

$$y = \frac{5.597 \times 10^6 \times \rho}{5.597 \times 10^6 \times \rho + \dfrac{177.28}{\sigma}} \times 100 \qquad [3]$$

where y = percentage of the total resistance between the contact points that is due to the carbon interconnects (the percentage of the voltage drop that occurs within the carbon interconnects), ρ = resistivity of the carbon, σ = conductivity of the medium.

By simplifying a system into a single equation, and creating a graph such as that shown in Fig. 12, a system designer could decide on parameters such as carbonization temperature, conductivity of

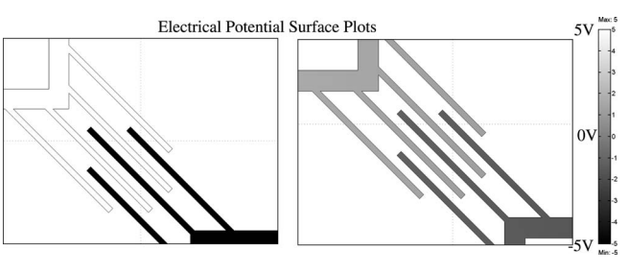

Figure 9. Simulation result (electrical potential surface plot) for SU-8 carbonized at 900°C submersed in a low conductivity medium (typical DI water) (left). The simulation result for the same structure immersed in a 0.8 S/m solution is shown on the right. ±5 V (10 V total) was applied to the ends of the left and right contact pads. Resistivity of carbon: 1.072×10^{-4} Ω m. Conductivity of medium: 10^{-4} S/m (left) and 0.8 S/m (right).

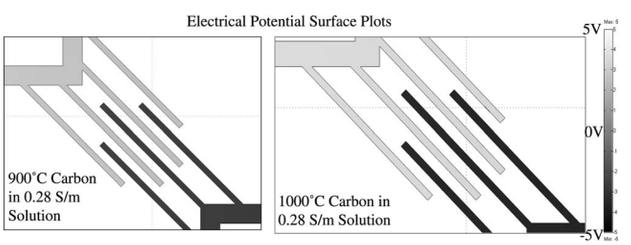

Figure 11. Simulation result (electrical potential surface plot) for SU-8 carbonized at 900°C submersed in a 0.28 S/m solution (typical conductivity for the electrolyte in a solid electrolyte Li-ion battery) (left). The simulation result for the same structure, but carbonized at 1000°C, is shown on the right. ±5 V (10 V total) was applied to the ends of the left and right contact pads. Resistivity of carbon: 1.072×10^{-4} Ω m (left) and 4.769×10^{-5} Ω m (right). Conductivity of medium: 0.28 S/m.

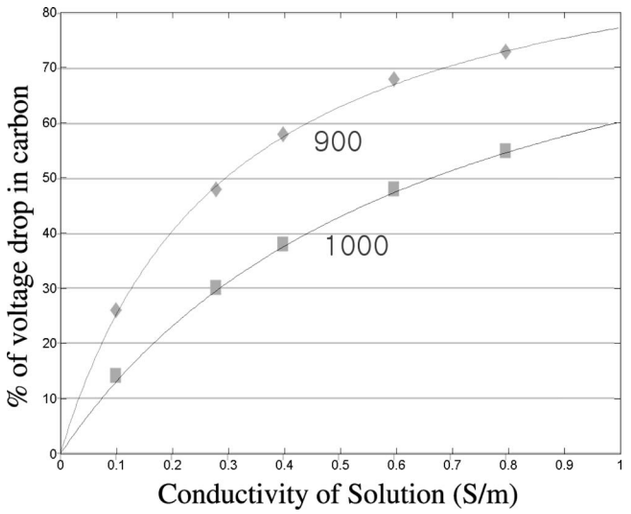

Figure 12. This figure shows that simplification of a whole C-MEMS/conductive medium system into a single equation by reducing it into a simple resistive network can be used to optimize a design to a certain application.

solution, and voltage applied for his/her system. The equation and graph can also be used to verify whether an existing design will work.

Conclusion

Electrical changes and shrinkage in various-thickness SU-8 and AZ P4620 photoresist-derived carbon carbonized at temperatures between 600 and 1000°C have been investigated. The sheet resistance and resistivity curves vs carbonization temperature were obtained. The electrical characteristics of the films carbonized at 1000°C seem to be similar regardless of resist type or thickness. The resistivity of samples measured at 1000°C was $5.330 \pm 0.574 \times 10^{-5}$ Ω m, regardless of resist type or film thickness. Thickness dependence in resistivity measurements performed on samples carbonized at lower temperatures was observed. This may be due to vertical heterogeneity of electrical properties within the films and/or the effects of thickness on the carbonization rate. Film shrinkage for the different samples was measured, and most of the reduction in thickness was found to happen at temperatures lower than 600°C. The AZ P4620-derived films showed no significant decrease in thickness between the temperatures of 600 and 1000°C, while the SU-8-derived carbon films did exhibit a decrease in height. Further experimental validation is required to determine the exact mechanism of carbonization in SU-8 and AZ P4620-derived carbon films. Simulations results underscoring the consequences of resistivity for C-MEMS applications in conductive media have been presented. Finally, a method of characterization of C-MEMS electrical systems in conductive media into simple mathematical formulas has been introduced.

Acknowledgments

All of the experimental work was done at the UCI Integrated Nanosystems Research Facility. This work was supported in part by National Science Foundation Contract DMI-0428958 through Mechanical and Aerospace Engineering, University of California, Irvine.

University of California, Irvine assisted in meeting the publication costs of this article.

References

1. C. L. Mantell, *Carbon and Graphite Handbook*, pp. 72–105, 247–288, 323–377, Interscience Publishers, New York (1968).
2. W. Benzinger, A. Becker, and K. J. Hüttinger, *Carbon*, **34**, 957 (1996).
3. D. B. Murphy, R. W. Carroll, and J. E. Klonowski, *Carbon*, **35**, 1819 (1997).
4. R. Shi, H. J. Li, Z. Yang, and M. K. Kang, *Carbon*, **35**, 1789 (1997).
5. O. Vohler, P. L. Reiser, and E. Sperk, *Carbon*, **6**, 397 (1968).
6. A. Becker and K. J. Hüttinger, *Carbon*, **36**, 201 (1998).
7. A. Becker and K. J. Hüttinger, *Carbon*, **36**, 177 (1998).
8. W. Benzinger and K. J. Hüttinger, *Carbon*, **34**, 1465 (1996).
9. C. L. Beyler and Marcelo M. Hirschler, in *SFPE Handbook of Fire Protection Engineering*, 3rd ed., P. J. DiNenno, Editor, NFPA, Quincy, MA (2001).
10. A. M. Lyons, C. W. Wilkins, and M. Robbins, *Thin Solid Films*, **103**, 333 (1983).
11. S. Ranganathan, R. McCreery, S. M. Majji, and M. Madou, *J. Electrochem. Soc.*, **147**, 277 (2000).
12. R. N. Basu, O. Altin, M. J. Mayo, C. A. Randall, and S. Eser, *J. Electrochem. Soc.*, **148**, A506 (2001).
13. G. M. Jenkins, *Clin. Phys. Physiol. Meas.*, **1**, 171 (1980).
14. J. C. Bokros, *Ceram. Int.*, **9**, 3 (1983).
15. A. Lyons, *J. Non-Cryst. Solids*, **70**, 99 (1985).
16. M. Madou, A. Lal, G. Schmidt, X. Song, K. Kinoshita, M. Fendorf, A. Zettl, and R. White, in *Chemical and Biological Sensors and Analytical Electrochemical Methods*, PV 97-19, p. 61–69, The Electrochemical Society Proceedings Series, Pennington, NJ (1997).
17. J. Kim, X. Song, K. Kinoshita, M. Madou, and R. White, *J. Electrochem. Soc.*, **145**, 2314 (1998).
18. R. Kostecki, B. Schnyder, D. Alliata, X. Song, K. Kinoshita, and R. Kotz, in *Chemical and Biological Sensors and Analytical Electrochemical Methods*, PV 97-19, p. 61–69, The Electrochemical Society Proceedings Series, Pennington, NJ (1997).
19. A. Singh, J. Jayaram, M. Madou, and S. Akbar, *J. Electrochem. Soc.*, **149**, E78 (2002).
20. C. Wang, G. Jia, L. H. Taherabadi, and M. J. Madou, *J. Microelectromech. Syst.*, **14**, 348 (2005).
21. L. Taherabadi, B. Y. Park, C. Wang, and M. Madou, *IEEE JMEMS*, Submitted.
22. C. Wang, L. Taherabadi, G. Jia, and M. Madou, *Electrochem. Solid-State Lett.*, **7**, A435 (2004).
23. B. Y. Park, R. Zaouk, and M. Madou, in *SPIE Microlithography*, Emerging Lithographic Technologies VIII, SPIE-The International Society for Optical Engineering, Bellingham, WA (2004).
24. K. Kinoshita, *Carbon, Electrochemical and Physicochemical Properties*, J. Wiley & Sons, New York (1988).
25. Clariant AZ P4000 Thick Film Photoresist Datasheet.
26. Microchem SU-8 data sheets.
27. F. M. Smits, *Bell Syst. Tech. J.*, **37**, 711 (1958).
28. R. F. Pierret, "Modular series on solid state devices," in *Semiconductor Fundamentals*, 2nd Ed., Vol. 1, Addison-Wesley Pub. Co., Inc., Reading, MA (1988).
29. L. J. Meng, T. Ibuki, M. Sakai, and Y. Hishiyama, *Carbon*, **29**, 1239 (1991).
30. L. H. Lee, *J. Polym. Sci., Part A: Gen. Pap.*, **3**, 859 (1965).
31. E. Fitzer and W. Schäfer, *Carbon*, **8**, 353 (1970).
32. A. Bürger, E. Fitzer, M. Heym, and B. Terwiesch, *Carbon*, **13**, 149 (1975).
33. Calculated using data from: V. Srinivasan and C. Y. Wang, *J. Electrochem. Soc.*, **150**, A98 (2003).
34. P.-H. Chang and M. M. Labes, *Chem. Mater.*, **1**, 523 (1989).
35. A. B. Kaufman, *Appl. Phys. Lett.*, **21**, 1 (1972).
36. H. Yasujima, M. Murakami, and S. Yoshimura, *Appl. Phys. Lett.*, **49**, 1 (1986).
37. L. D. Woolf, J. Chin, Y. R. Lin Liu, and H. Ikezi, *Phys. Rev. B*, **30**, 861 (1984).
38. O. J. A. Schueller, S. T. Brittain, and G. M. Whitesides, *Sens. Actuators, A*, **72**, 125 (1999).
39. C. L. Renschler, A. P. Sylwester, and L. V. Salgado, *J. Mater. Res.*, **4**, 452 (1989).
40. O. Niwa and H. Tabel, *Anal. Chem.*, **66**, 285 (1994).
41. R. Schlesinger, M. Bruns, and H.-J. Ache, *J. Electrochem. Soc.*, **144**, 6 (1997).